



Joint-Mapping Orthogonal Frequency Division Multiplexing with Subcarrier Number Modulation

Item Type	Article
Authors	Wen, Miaowen; Li, Jun; Dang, Shuping; Lia, Qiang; Mumtaz, Shahid; Arslan, Huseyin
Citation	Wen, M., Li, J., Dang, S., Lia, Q., Mumtaz, S., & Arslan, H. (2021). Joint-Mapping Orthogonal Frequency Division Multiplexing with Subcarrier Number Modulation. IEEE Transactions on Communications, 1-1. doi:10.1109/tcomm.2021.3066584
Eprint version	Post-print
DOI	10.1109/TCOMM.2021.3066584
Publisher	Institute of Electrical and Electronics Engineers (IEEE)
Journal	IEEE Transactions on Communications
Rights	(c) 2021 IEEE. Personal use of this material is permitted. Permission from IEEE must be obtained for all other users, including reprinting/ republishing this material for advertising or promotional purposes, creating new collective works for resale or redistribution to servers or lists, or reuse of any copyrighted components of this work in other works.
Download date	09/08/2022 07:29:03
Link to Item	http://hdl.handle.net/10754/668180

Joint-Mapping Orthogonal Frequency Division Multiplexing with Subcarrier Number Modulation

Miaowen Wen, *Senior Member, IEEE*, Jun Li, *Member, IEEE*, Shuping Dang, *Member, IEEE*, Qiang Li, *Member, IEEE*, Shahid Mumtaz, *Senior Member, IEEE* and Huseyin Arslan, *Fellow, IEEE*

Abstract—Orthogonal frequency division multiplexing with subcarrier number modulation (OFDM-SNM) has been recently proposed to improve the spectral efficiency (SE) of the traditional OFDM system. In this paper, we propose a joint-mapping OFDM-SNM (JM-OFDM-SNM) scheme to transmit the signal vector with a constant length of information bits by jointly considering the subcarrier activation patterns and constellation symbols. A low-complexity detection scheme based on log-likelihood ratio criterion is proposed to relieve the high computational complexity of the maximum-likelihood detection at the cost of a negligible performance loss. Upper-bounded bit error rate (BER) and lower-bounded achievable rate are both derived in closed-form to evaluate the performance of JM-OFDM-SNM. To suit different application scenarios, we further propose two enhanced schemes, named adaptive JM-OFDM-SNM (AJM-OFDM-SNM) and JM-OFDM with in-phase/quadrature SNM (JM-OFDM-IQ-SNM), where the former adjusts the constellation orders for different numbers of active subcarriers, and the latter extends the indexing to in-phase and quadrature domains. Simulation results corroborate the tightness of the derived BER expression in the high signal-to-noise ratio region and show that (A)JM-OFDM-SNM improves the performance of OFDM-SNM, while both AJM-OFDM-SNM and JM-OFDM-IQ-SNM schemes perform better than JM-OFDM-SNM at the same SE.

Index Terms—Orthogonal frequency division multiplexing (OFDM), subcarrier number modulation, bit error rate (BER), joint mapping, low-complexity detection.

I. INTRODUCTION

INDEX modulation (IM) is a class of modulation techniques that enjoy high spectral efficiency (SE) and energy efficiency (EE) [1]–[4]. In IM, the index(es) of the patterns, such as

This work was supported in part by National Nature Science Foundation of China under Grants 61871190 and 61872102, in part by the International Collaborative Research Program of Guangdong Science and Technology Department under Grant No. 2020A0505100061, in part by the Natural Science Foundation of Guangdong Province under Grant 2018B030306005, in part by the Open Research Fund of the National Mobile Communications Research Laboratory, Southeast University under Grant 2020D03, and in part by the Fundamental Research Funds for the Central Universities under Grant 2019SJ02. (*Corresponding author: Jun Li*)

Miaowen Wen is with the School of Electronic and Information Engineering, South China University of Technology, Guangzhou 510641, China, and also with the National Mobile Communications Research Laboratory, Southeast University, Nanjing 210096, China (e-mail: eemwwen@scut.edu.cn).

Jun Li is with Research Center of Intelligent Communication Engineering, School of Electronics and Communication Engineering, Guangzhou University, Guangzhou 510006, China (e-mail: lijun52018@gzhu.edu.cn).

Shuping Dang is with Computer, Electrical and Mathematical Science and Engineering Division, King Abdullah University of Science and Technology (KAUST), Thuwal 23955-6900, Kingdom of Saudi Arabia (e-mail: shuping.dang@kaust.edu.sa).

Qiang Li is with the College of Information Science and Technology, Jinan University, Guangzhou 510632, China (e-mail: qiangli@jnu.edu.cn).

Shahid Mumtaz is with the Instituto de Telecomunicacoes, 112148 Lisboa, Portugal, and also with ARIES Research Center, Universidade Antonio de Nebrija, C/Pirineos, 55, E-28040, Madrid, Spain (e-mail: smumtaz@av.it.pt).

Huseyin Arslan is with the Department of Electrical Engineering, University of South Florida, Tampa, FL 33620 USA (e-mail: arslan@usf.edu).

active transmit antennas, receive antennas, time slots, orthogonal frequency division multiplexing (OFDM) subcarriers, and spreading codes, are encoded by extra information bits for transmission [5]–[7].

The IM concept was first applied to the space domain, generating spatial modulation (SM) [8]. Unlike the conventional multiple-input multiple-output (MIMO) schemes, the information bits of SM are divided into index bits and modulation bits, where the former determine a single active transmit antenna, and the latter generate a modulated symbol to be transmitted via it. SM has many benefits due to the activation of only a single transmit antenna, including high EE, free inter-channel interference, and free synchronization. Soon after SM, space shift keying (SSK) was proposed as a special case of SM by transmitting the index of the active transmit antenna only [9]. Although SM and SSK have high EE, their SEs are relatively low compared to that of MIMO schemes. Therefore, generalized SM (GSM) [10], [11] and generalized SSK (GSSK) [12] were proposed to improve the SEs of SM and SSK systems, respectively, which allow activating multiple transmit antennas. In [13], quadrature SM (QSM) was proposed as another means to increase the SE of SM systems by extending the indexing to the in-phase and quadrature (IQ) domains. As a different way to realize IM in the space domain, antenna number modulation (ANM) was proposed in [14] to convey the index bits by changing the number of active transmit antennas, which shows better performance than SM. It is worth noting that only the indices of transmit antennas are used in the aforementioned studies. Contrarily, the indices of receive antennas were first used to convey index bits by so-called precoding SM (PSM) in [15]. In virtue of the pre-coding technique, PSM can outperform SM. Because of this, several works related to PSM have been proposed [16]–[18]. In [16], generalised PSM (GPSM) was proposed to increase the SE of PSM systems by activating multiple receive antennas. The performance of the multi-stream GPSM scheme was analyzed in [17]. To further increase the SE, generalised pre-coding QSM (GPQSM) was proposed to merge GPSM with QSM in [18].

In parallel with the fast development of IM in the space domain, the IM concept has been also actively applied to the frequency domain. In [19], OFDM with IM (OFDM-IM) was proposed to transmit the subcarrier activation pattern (SAP) as well as the modulated symbols via the active subcarriers. It was shown that OFDM-IM has the potential to outperform the conventional OFDM scheme. Attracted by the merits of OFDM-IM, a number of researchers have been engaged to unlock the potential of OFDM-IM. The interleaved subcarrier grouping method was proposed for OFDM-IM systems to

harvest the frequency diversity [20], [21]. Enhanced OFDM-IM was proposed to enhance the bit error rate (BER) performance of OFDM-IM systems by extending the indexing to in-phase/quadrature domains (similar to QSM) [22]. A special constellation design was proposed in [23] by activating all SAPs for transmission. To increase the SE of OFDM-IM systems, a generalized OFDM-IM scheme was proposed to enlarge the number of index bits in [24]. For the same purpose, the authors of [25] proposed a layered OFDM-IM scheme by selecting SAPs via multiple layers, and OFDM-IM was even combined with MIMO [26]. All above-mentioned OFDM-IM related schemes only activate a fraction of subcarriers at each OFDM symbol duration, which wastes the frequency resource and limits the increase of SE. In order to break this limit, dual-mode IM aided OFDM (DM-IM-OFDM) and its generalization were proposed to utilize both selected and unselected subcarriers to transmit modulated symbols [27], [28]. Moreover, the authors of [29] and [30] also designed multiple-mode (MM-)OFDM-IM and its generalization to transmit modulated symbols via a full set of subcarriers. While DM-IM-OFDM maps index bits to the indices of selected subcarriers, MM-OFDM-IM encodes the full permutation of multiple distinguishable constellations. On the other hand, OFDM with subcarrier power modulation (OFDM-SPM) was proposed to convey index bits via different powers of all subcarriers [31], [32]. Except for improving the SE, the design of low-complexity detectors is also critical for OFDM-IM family [33]–[35].

Despite many advantages, OFDM-IM and its variants mentioned above still have some deficiencies. For example, they transmit their own signal through a fixed number of active subcarriers, which has not fully exploited the SE advantage of IM. Furthermore, the mapping between index bits and SAP becomes very complex when the number of subcarriers goes large. To solve these problems, OFDM with subcarrier number modulation (OFDM-SNM) was proposed to convey index bits via the number of subcarriers [36]–[38]. In OFDM-SNM, the number of active subcarriers is no longer fixed, achieving a higher SE than OFDM-IM under certain conditions. Nevertheless, the length of information bits of OFDM-SNM is varied depending on the number of active subcarriers, which may lead to error propagation, and make the scheduling and resource allocation challenging. To solve the underlying problems of OFDM-SNM, in this paper we propose a joint-mapping (JM-)OFDM-SNM to generate a constant length of information bits for each transmission. In JM-OFDM-SNM, the transmitted vectors are generated by considering all possible SAPs and corresponding modulated symbols. Then, a bijective mapping is implemented based on the information bits. A low-complexity near-optimal detection method based on log-likelihood ratio (LLR) criterion is proposed to relieve the high detection load of the optimal maximum-likelihood (ML) detection. Theoretical analysis for upper bounded BER and lower bounded achievable rate of JM-OFDM-SNM systems is also performed, both of which are derived in closed-form. Noticing that the number of transmitted vectors for JM-OFDM-SNM is not always a power of two, and a portion of transmitted vectors are unused, which affects the transmission

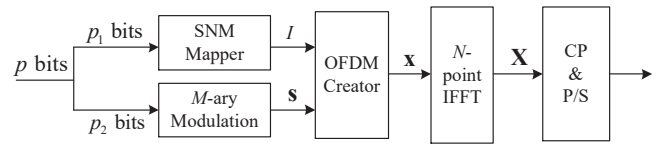


Fig. 1. System model of OFDM-SNM.

rate and BER performance of JM-OFDM-SNM, we further propose two enhanced JM-OFDM-SNM schemes as possible remedies. The first one is called adaptive JM-OFDM-SNM (AJM-OFDM-SNM), which selects the modulated symbols from different signal constellations for different numbers of active subcarriers. By properly adjusting the constellation sizes, AJM-OFDM-SNM obtains a better BER performance and a higher transmission rate than JM-OFDM-SNM. The second one is called JM-OFDM with in-phase/quadrature SNM (JM-OFDM-IQ-SNM), which extends the indexing to the IQ domains. Due to the domain extension, JM-OFDM-IQ-SNM generates more transmitted vectors than JM-OFDM-SNM, and hence a higher transmission rate. Simulation results corroborate the tightness of the derived BER upper bound at high signal-to-noise ratio (SNR), and show that (A)JM-OFDM-SNM obtains a better BER performance than OFDM-SNM and conventional OFDM at the same transmission rate. Moreover, both proposed enhanced schemes achieve better BER performance than JM-OFDM-SNM.

The rest of this paper is organized as follows. In Section II, we introduce the conventional OFDM-SNM scheme. The proposed JM-OFDM-SNM scheme as well as its low-complexity LLR detection method are proposed in Section III. The BER and achievable rate of JM-OFDM-SNM are analyzed in Section IV. Section V proposes the two enhanced JM-OFDM-SNM schemes, namely AJM-OFDM-SNM and JM-OFDM-IQ-SNM. Simulation results are presented and discussed in Section VI. Finally, this paper is concluded in Section VII.

Notations: Upper and lower case boldface letters denote matrices and column vectors, respectively. The complex number field is represented by \mathbb{C} . $(\cdot)^T$ and $(\cdot)^H$ represent the transpose and Hermitian transpose operations, respectively. \mathbf{I}_M is an $M \times M$ identity matrix. $E\{\cdot\}$ denotes the expectation operation. $\|\cdot\|$ denotes the Frobenius norm. $C(\cdot, \cdot)$ represent the binomial operation. $Q(\cdot)$ denotes the Gaussian Q -function. $\text{rank}\{\cdot\}$ indicates the rank of the argument. $\text{diag}\{\mathbf{x}\}$ denotes a diagonal matrix whose diagonal elements are drawn from \mathbf{x} . $\det\{\cdot\}$ represents the determinant. The probability of an event is denoted by $\Pr(\cdot)$. $\lfloor \cdot \rfloor$ indicates the floor operation. $\max(\cdot, \cdot)$ denotes the maximum operation of two arguments.

II. CONVENTIONAL OFDM-SNM SCHEME REVISITED

The system model of OFDM-SNM with totally N subcarriers is depicted in Fig. 1. In OFDM-SNM, p input bits are split into two parts, i.e., index bits (p_1 bits) determining a certain number of active subcarriers, and modulation bits (p_2 bits) generating M -ary phase shift keying (PSK) or quadrature amplitude modulation (QAM) symbols. In mathematical representation, the first part of $p_1 = \log_2(N)$ bits selects one out of N SAPs $I = [1, \dots, 1, 0, \dots, 0]$ with $l(\in \{1, \dots, N\})$ ones

based on a certain mapping rule (e.g., see Table I with $N = 4$), indicating that the first l subcarriers are activated. The second part of $p_2 = l \log_2(M)$ bits generates l modulated symbols $\mathbf{s} = [s_1, s_2, \dots, s_l]$, where $s_\alpha \in \mathcal{S}$ with $\alpha \in \{1, \dots, l\}$ and \mathcal{S} denoting the M -ary constellation. It is worth noting that the length of modulation bits p_2 is varied due to the variable value of l . Therefore, the length of input bits $p = p_1 + p_2$ is also varied. The average transmission rate of OFDM-SNM in bit per channel use (bpcu), can be calculated by

$$\bar{r}_{\text{SNM}} = \log_2(N) + \frac{1+N}{2} \log_2(M). \quad (1)$$

After obtaining I and \mathbf{s} , the OFDM transmitted vector \mathbf{x} in the frequency domain can be expressed as

$$\mathbf{x} = [s_1, s_2, \dots, s_l, 0, \dots, 0]^T. \quad (2)$$

TABLE I
MAPPING TABLE OF OFDM-SNM WITH $N = 4$ AND $p_1 = 2$.

l	p_1	SAP I	l	p_1	SAP I
1	00	[1, 0, 0, 0]	2	01	[1, 1, 0, 0]
3	10	[1, 1, 1, 0]	4	11	[1, 1, 1, 1]

For clarity and illustration purposes, we give an example for OFDM-SNM with $N = 4$ and BPSK ($M = 2$). Assume a case that the input bits are (0110). Based on Table I, the first two bits (01) select the SAP $I = [1, 1, 0, 0]$ with $l = 2$. The second two bits (10) generate modulated symbols $\mathbf{s} = [+1, -1]$. Therefore, the OFDM transmitted vector can be expressed by $\mathbf{x} = [+1, -1, 0, 0]^T$. Let us see another case in which the input bits become (10110). Similarly, the first two bits (10) select the SAP $I = [1, 1, 1, 0]$ with $l = 3$, and the second three bits (110) generate modulated symbols $\mathbf{s} = [+1, +1, -1]$. The OFDM transmitted vector is then given by $\mathbf{x} = [+1, +1, -1, 0]^T$. It is clear from above two cases that although OFDM-SNM has the same length of index bits ($p_1 = 2$), the lengths of modulation bits are different (one is 2 and the other is 3) due to different SAPs with different numbers of active subcarriers, resulting in different lengths of the input bits.

Having the OFDM transmitted vector \mathbf{x} , the N -point inverse fast Fourier transform (IFFT) is applied to generate the time-domain OFDM signal as

$$\mathbf{X} = [X_1, X_2, \dots, X_N]^T. \quad (3)$$

Finally, the OFDM signal is transmitted to the receiver side after appending the cyclic prefix (CP) to the beginning of \mathbf{X} and parallel to serial (P/S) conversion.

III. PROPOSED JM-OFDM-SNM SCHEME

OFDM-SNM has a variable length of input bits, which may incur error propagation. To solve this problem, we propose JM-OFDM-SNM, which maintains a constant length of input bits.

A. Working Principle

In JM-OFDM-SNM, V subcarriers are allowed to be activated with $V \in \{1, \dots, N\}$. Similar to OFDM-SNM, the number of active subcarriers is varied. However, unlike the

mapping strategy that relates the SAP with the index bits only in OFDM-SNM, JM-OFDM-SNM performs a joint mapping between the input bits and the transmitted vectors. In JM-OFDM-SNM, there are totally $N_T = \sum_{v=1}^V C(N, v)$ SAPs. For each SAP $I = [i_1, \dots, i_v]$, v subcarriers are active, such that v modulated symbols $\mathbf{s} = [s_1, \dots, s_v]$ can be transmitted via them. Considering all candidates for v subcarriers and modulated symbols, the number of all possible transmitted vectors can be calculated as

$$N_A = \sum_{v=1}^V C(N, v) M^v. \quad (4)$$

Since the total number of transmitted vectors N_A is fixed, a constant length of input bits (m bits) for JM-OFDM-SNM can be obtained by a bijective mapping between input bits and N_A transmitted vectors, which results in an SE of

$$\bar{r}_{\text{JM}} = m = \lfloor \log_2(N_A) \rfloor. \quad (5)$$

Note that N_A may not be a power of two, and in such cases only $F = 2^{\lfloor \log_2(N_A) \rfloor}$ transmitted vectors are used for transmission.

Similarly, the OFDM transmitted vector for JM-OFDM-SNM in the frequency domain can be obtained by combining I and \mathbf{s} as

$$\mathbf{x}_k = [0, \dots, s_1, \dots, 0, \dots, s_2, \dots, 0, \dots, s_v, \dots, 0]^T, \quad (6)$$

where $k \in \{1, \dots, F\}$.

TABLE II
MAPPING TABLE OF JM-OFDM-SNM WITH $N = 4$, $V = 3$ AND BPSK.

v	k	Input Bits	\mathbf{x}_k
1	1	000000	$[-1, 0, 0, 0]^T$
1	2	000001	$[+1, 0, 0, 0]^T$
\vdots	\vdots	\vdots	\vdots
2	31	011110	$[0, 0, +1, -1]^T$
2	32	011111	$[0, 0, +1, +1]^T$
\vdots	\vdots	\vdots	\vdots
3	63	111110	$[0, +1, +1, -1]^T$
3	64	111111	$[0, +1, +1, +1]^T$

We provide an example of JM-OFDM-SNM for illustration with $N = 4$, $V = 3$, and BPSK. In this case, there are totally $N_A = \sum_{v=1}^3 C(4, v) 2^v = 64$ possible transmitted vectors, which lead to totally 6 input bits ($m = 6$). The corresponding mapping table is given in Table II. From Table II, the transmitted vector \mathbf{x}_k can be directly obtained by certain input bits. For instance, assume the input bits are (011110) with $k = 31$. The corresponding transmitted vector is given by $\mathbf{x}_{31} = [0, 0, +1, -1]^T$. However, if the input bits are (000001) with $k = 2$, the transmitted vector is then obtained as $\mathbf{x}_2 = [+1, 0, 0, 0]^T$.

Compared with the conventional OFDM-SNM, JM-OFDM-SNM achieves a constant length of input bits, which avoids

the error propagation. Moreover, not all subcarriers need to be activated for transmission by JM-OFDM-SNM, which saves the transmit power. However, compared with the conventional OFDM-SNM scheme, the size of mapping table for JM-OFDM-SNM is relatively larger, which might lead to high search or detection complexity.

The subsequent process is the same as that of the conventional OFDM scheme. First, the N -point IFFT is applied to \mathbf{x}_k , resulting in time-domain signal $\mathbf{X}^k = [X_1^k, X_2^k, \dots, X_N^k]^T$. Then, it is transmitted to the receiver after CP insertion and P/S conversion.

At the receiver, the frequency-domain received signal vector can be expressed by

$$\mathbf{y} = \frac{1}{\sqrt{\bar{v}}} \mathbf{H} \mathbf{x}_k + \mathbf{n}, \quad (7)$$

where $\mathbf{H} = \text{diag}\{\mathbf{h}\} = \text{diag}\{[h_1, h_2, \dots, h_N]^T\}$ denotes the channel coefficient matrix whose entries follow the complex Gaussian distribution with zero mean and unit variance; \bar{v} denotes the average number of active subcarriers; \mathbf{n} represents the additive white Gaussian noise (AWGN) vector with zero mean and variance N_0 . The transmitted signal can be estimated by employing the optimal ML detection

$$\hat{\mathbf{x}}_k = \arg \min_{\mathbf{x}_k} \left\| \mathbf{y} - \frac{1}{\sqrt{\bar{v}}} \mathbf{H} \mathbf{x}_k \right\|^2. \quad (8)$$

It can be seen from (8) that the optimal ML detection requires an exhaustive search over all possible candidates for the transmitted vector \mathbf{x}_k , which results in high computational complexity, especially for large values of N , V , or M .

B. Low-Complexity Detection

In this subsection, we propose an LLR detection method, which largely reduces the computational complexity. The LLR metric can be formulated as

$$L(\alpha) = \ln \frac{\Pr(\mathbf{A}_\alpha | y(\alpha))}{\Pr(\bar{\mathbf{A}}_\alpha | y(\alpha))} = \ln \frac{\Pr(\mathbf{A}_\alpha) f(y(\alpha) | \mathbf{A}_\alpha)}{\Pr(\bar{\mathbf{A}}_\alpha) f(y(\alpha) | \bar{\mathbf{A}}_\alpha)}, \quad (9)$$

where $y(\alpha)$ stands for the α th element of \mathbf{y} , \mathbf{A}_α denotes the event that the α th subcarrier is active of probability $\Pr(\mathbf{A}_\alpha) = \frac{1}{NT} \sum_{v=1}^V vC(N, v)$ with $T = \sum_{v=1}^V C(N, v)$, and $\bar{\mathbf{A}}_\alpha$ represents the complementary event of \mathbf{A}_α with $\Pr(\bar{\mathbf{A}}_\alpha) = 1 - \Pr(\mathbf{A}_\alpha)$. The conditional probability density function (PDF) $f(y(\alpha) | \mathbf{A}_\alpha)$ can be explicitly expressed in (10), shown at the top of the next page. In (10), we have adopted an estimation of the PDF when considering the α th subcarrier to be active. In fact, the exact PDF should take into account the appearance probability of each constellation point. However, to reduce the computational complexity we only keep the constellation point $\hat{s}(\alpha)$ that is associated with the minimum Euclidean distance.

After calculating all values of $L(\alpha)$, $\alpha = 1, \dots, N$, we obtain the LLR vector

$$\mathbf{L} = [L(1), \dots, L(N)],$$

and the correspondingly estimated modulated symbols $\hat{\mathbf{s}} = [\hat{s}_1, \dots, \hat{s}_N]$. It can be seen from (9) that the α th subcarrier is more likely to be activated with a larger value of $L(\alpha)$. In order to figure out the possible number and the corresponding

indices of active subcarriers, we first sort the values of \mathbf{L} as $[z_1, \dots, z_N] = \text{sort}([L(1), \dots, L(N)])$, where $\text{sort}(\cdot)$ denotes the ordering function that reorders the elements in descending order, and z_1 (z_N) denotes the position of the maximum (minimum) value in \mathbf{L} . Therefore, the V possible SAPs can be estimated as

$$\hat{I}_1 = [z_1], \hat{I}_2 = [z_1, z_2], \dots, \hat{I}_V = [z_1, \dots, z_V], \quad (11)$$

where \hat{I}_v indicates the estimated SAP for activating v subcarriers with $v \in \{1, \dots, V\}$. To find the final estimate of SAP (or the number of active subcarriers v), we need to further compare the Euclidean distances of all V possible SAPs as follows:

$$\hat{v} = \arg \min_{\{\hat{I}_v\}_{v=1, \dots, V}} \left\| \mathbf{y} - \frac{1}{\sqrt{\bar{v}}} \mathbf{H} \mathbf{x}'_v \right\|^2, \quad (12)$$

where $\mathbf{x}'_v = [0, \dots, \hat{s}_1, \dots, 0, \dots, \hat{s}_v, \dots, 0]^T$ with the non-zero elements in the positions of \hat{I}_v . After obtaining \hat{v} , the estimated signal vector $\hat{\mathbf{x}}$ can be directly constructed by $\hat{I}_{\hat{v}}$ and $\hat{\mathbf{s}}$. Finally, the information bits are extracted by demapping $\hat{\mathbf{x}}$.

IV. PERFORMANCE ANALYSIS AND DESIGN GUIDELINES

A. BER Upper Bound

In this subsection, we theoretically deduce an upper bound on the BER of JM-OFDM-SNM, assuming perfect channel state information at the receiver.

The detection error comes from the SAP detection and/or symbol detection, which leads to BER of

$$P_e \approx \frac{1}{2} P_I + \frac{b P_b}{m} (1 - P_I), \quad (13)$$

where b is the average number of modulation bits with

$$b = \log_2(M) \frac{\sum_{v=1}^V v C(N, v)}{\sum_{v=1}^V C(N, v)}, \quad (14)$$

and P_I denotes the error probability of detecting the SAP I , which can be derived according to the union bounding technique as [40]

$$P_I \leq \frac{1}{F} \sum_{\mathbf{x}_k} \sum_{\hat{\mathbf{x}}_k, I \neq \hat{I}} \Pr\{\mathbf{x}_k \rightarrow \hat{\mathbf{x}}_k\}, \quad (15)$$

with $\Pr\{\mathbf{x}_k \rightarrow \hat{\mathbf{x}}_k\}$ representing the unconditional pairwise error probability (PEP). In order to obtain $\Pr\{\mathbf{x}_k \rightarrow \hat{\mathbf{x}}_k\}$, we first calculate the conditional PEP on \mathbf{H} , which is given by

$$\begin{aligned} \Pr\{\mathbf{x}_k \rightarrow \hat{\mathbf{x}}_k | \mathbf{H}\} &= \Pr\left\{ \left\| \mathbf{y} - \frac{\mathbf{H} \mathbf{x}_k}{\sqrt{\bar{v}}} \right\|^2 > \left\| \mathbf{y} - \frac{\mathbf{H} \hat{\mathbf{x}}_k}{\sqrt{\bar{v}}} \right\|^2 \right\} \\ &= Q\left(\sqrt{\frac{\|\mathbf{H}(\mathbf{x}'_k - \hat{\mathbf{x}}'_k)\|^2}{2N_0}} \right), \end{aligned} \quad (16)$$

where $\mathbf{x}'_k = \mathbf{x}_k / \sqrt{\bar{v}}$ and $\hat{\mathbf{x}}'_k = \hat{\mathbf{x}}_k / \sqrt{\bar{v}}$. Applying the Q -function approximation [39]

$$Q(x) \cong \frac{1}{12} e^{-\frac{x^2}{2}} + \frac{1}{4} e^{-\frac{2x^2}{3}}, \quad (17)$$

$$f(y(\alpha)|\mathbf{A}_\alpha) = \begin{cases} \frac{1}{\pi N_0} \exp(-\frac{1}{N_0}|y(\alpha) - \frac{1}{\sqrt{v}}h_\alpha \hat{s}(\alpha)|^2), & \text{if the } \alpha\text{th subcarrier is active,} \\ \frac{1}{\pi N_0} \exp(-\frac{1}{N_0}|y(\alpha)|^2), & \text{if the } \alpha\text{th subcarrier is inactive.} \end{cases} \quad (10)$$

the unconditional PEP can be approximated as

$$\Pr\{\mathbf{x}_k \rightarrow \hat{\mathbf{x}}_k\} = E_{\mathbf{H}} \{\Pr\{\mathbf{x}_k \rightarrow \hat{\mathbf{x}}_k|\mathbf{H}\}\} \\ = \frac{1/12}{\det(\mathbf{I}_N + q_1 \mathbf{K} \mathbf{A})} + \frac{1/4}{\det(\mathbf{I}_N + q_2 \mathbf{K} \mathbf{A})}, \quad (18)$$

where $\mathbf{A} = \text{diag}\{\mathbf{x}'_k - \hat{\mathbf{x}}'_k\}^H \text{diag}\{\mathbf{x}'_k - \hat{\mathbf{x}}'_k\}$; $\mathbf{K} = E\{\mathbf{H}\mathbf{H}^H\}$ is the covariance matrix of \mathbf{H} ; $q_1 = 1/(4N_0)$ and $q_2 = 1/(3N_0)$. Substituting (18) into (15), an upper bound of P_I can be obtained.

On the other hand, P_b denotes error probability of symbol detection, which is given by [41]

$$P_b \cong \frac{2}{\max(\log_2(M), 2)} \sum_{i=1}^{\max(M/4, 1)} \frac{1}{2} \\ \times \left(1 - \sqrt{\frac{\sin^2\left(\frac{(2i-1)\pi}{M}\right)}{\bar{v}N_0 + \sin^2\left(\frac{(2i-1)\pi}{M}\right)}} \right), \quad \text{for PSK,} \quad (19)$$

and

$$P_b = \frac{1}{\log_2(\sqrt{M})} \sum_{m=1}^{\log_2(\sqrt{M})} P_b(m), \quad \text{for QAM,} \quad (20)$$

where

$$P_b(t) = \frac{2}{\sqrt{M}} \sum_{i=0}^{(1-2^{-t})\sqrt{M}-1} \\ \times \{(-1)^{\lfloor \frac{i \cdot 2^{t-1}}{\sqrt{M}} \rfloor} \left(2^{t-1} - \left\lfloor \frac{i \cdot 2^{t-1}}{\sqrt{M}} + \frac{1}{2} \right\rfloor \right) p(i)\}, \quad (21)$$

with

$$p(i) = \frac{1}{2} \left(1 - \sqrt{\frac{\frac{3(2i+1)^2}{2(M-1)\bar{v}N_0}}{1 + \frac{3(2i+1)^2}{2(M-1)\bar{v}N_0}}} \right). \quad (22)$$

B. Guidelines for Transmitted Vector Selection

When N_A is not a power of two, which is the general case, only $F = 2^{\lfloor \log_2(N_A) \rfloor}$ transmitted vectors are used for JM-OFDM-SNM, which implies that a different selection of F transmitted vectors may affect the system performance. Therefore, we provide a guideline for transmitted vector selection in this subsection.

First, we should consider the complexity of mapping between information bits and selected combination vectors. If the number of all transmitted vectors N_A is small, it is easy to optimally select F transmitted vectors and build the mapping between information bits and the optimal F transmitted vectors via a well-designed look-up table. However, it is very difficult to optimally select F transmitted vectors if N_A goes large. Furthermore, it is also very difficult to build the mapping between the information bits and F transmitted vectors.

Therefore, to facilitate the mapping between the information bits and the selected combination vectors, we assume that the latter are determined from the consecutive F vectors among all N_A transmitted vectors.

We can see from (13) that P_e is dominated by P_b and P_I . While P_b is only related to M and \bar{v} , which is not affected by different combinations of possible transmitted vectors, it can be inferred from (15) and (18) that different combinations of transmitted vectors affect \mathbf{A} (or P_I), and hence the BER P_e . To further figure out the effect of different combinations of possible transmitted vectors, we provide an asymptotic analysis of P_I at high SNR in the sequel.

It can be seen from (18) that \mathbf{A} is a diagonal matrix with d nonzero eigenvalues $\lambda_1, \lambda_2, \dots, \lambda_d$. Note that \mathbf{K} becomes an identity matrix with sufficiently deep interleaving. Therefore, the unconditional PEP can be rewritten as

$$\Pr(\mathbf{x}_\alpha \rightarrow \hat{\mathbf{x}}_\alpha) \simeq \frac{1/12}{\prod_{t=1}^d (1 + q_1 \lambda_t)} + \frac{1/4}{\prod_{t=1}^d (1 + q_1 \lambda_t)}. \quad (23)$$

Assuming a rich scattering environment, (23) can be approximated at high SNR as

$$\Pr(\mathbf{x}_\alpha \rightarrow \hat{\mathbf{x}}_\alpha) \simeq \left(12q_1^d \prod_{t=1}^d \lambda_t \right)^{-1} + \left(4q_2^d \prod_{t=1}^d \lambda_t \right)^{-1}, \quad (24)$$

with $d = \min \text{rank}\{\mathbf{A}\} = 1$. It can be seen from (15) and (24) that P_I is smaller if the selected transmitted vector set contains a small number of any vector pair with $\text{rank}\{\mathbf{A}\} = 1$. In other words, the selected transmitted vector set leads to better performance with fewer cases satisfying “ $\text{rank}\{\mathbf{A}\} = 1$ ” by considering all transmitted vectors. In our paper, we select F transmitted vectors containing the smallest number of vector pairs with $\text{rank}\{\mathbf{A}\} = 1$.

C. Achievable Rate

We derive the achievable rate of the proposed JM-OFDM-SNM system according to the definition of mutual information between \mathbf{y} and \mathbf{x} , which is given by [21]

$$r = \frac{1}{N} I(\mathbf{x}; \mathbf{y}) = \frac{1}{N} (H(\mathbf{x}) - H(\mathbf{x}|\mathbf{y})) \\ = \frac{\bar{v}}{N} - \frac{1}{N} E_{\mathbf{h}} [H(\mathbf{x}|\mathbf{y}, \mathbf{h})]. \quad (25)$$

The conditional PDF of \mathbf{y} on \mathbf{x} and \mathbf{h} is given by

$$f(\mathbf{y}|\mathbf{x}, \mathbf{h}) = \frac{1}{(\pi N_0)^N} \exp(-\|\mathbf{y} - \frac{1}{\sqrt{v}} \text{diag}\{\mathbf{h}\}\mathbf{x}\|^2), \quad (26)$$

and that on \mathbf{h} is

$$f(\mathbf{y}|\mathbf{h}) = \frac{1}{F} \sum_{\varsigma=1}^F f(\mathbf{y}|\mathbf{x}_\varsigma, \mathbf{h}), \quad (27)$$

where \mathbf{x}_ς denotes the ς -th observation of \mathbf{x} . After carefully scrutinizing (26) and (27), we find no closed-form for (25).

Therefore, we resort to the lower-bounded technique proposed in [21] to obtain a lower bound on the achievable rate as

$$r \geq \frac{\bar{v}}{N} - (\log_2(e) - 1) - \frac{1}{NF} \sum_{\omega=1}^F \left(\log_2 \sum_{\eta=1}^F \frac{1}{\det(\mathbf{I}_N + \Xi_{\omega,\eta})} \right), \quad (28)$$

where $\Xi_{\omega,\eta} = \frac{1}{2N_0} \text{diag}\{\mathbf{x}_\omega - \mathbf{x}_\eta\}^H \text{diag}\{\mathbf{x}_\omega - \mathbf{x}_\eta\}$.

V. ENHANCED JM-OFDM-SNM

As can be seen from (4), the total number of all possible transmitted vectors N_A in JM-OFDM-SNM is usually not a power of two. Therefore, $N_A - F$ transmitted vectors would be discarded for modulation purposes, which leads to a vast waste of subcarrier resources and limits the transmission rate. In this section, we propose two enhanced JM-OFDM-SNM schemes, namely AJM-OFDM-SNM and JM-OFDM-IQ-SNM, to improve the transmission rate and BER performance of JM-OFDM-SNM, respectively.

A. AJM-OFDM-SNM

The AJM-OFDM-SNM scheme adaptively generates the modulated symbols from different constellations for different numbers of activated subcarriers (v). Specifically, in order to make full use of all N_A transmitted vectors, we can adapt the cardinality of the constellation for each v so as to achieve a higher transmission rate or a lower BER, which results in a total number of transmitted vectors

$$\bar{N}_A = \sum_{v=1}^V C(N, v)(M_v)^v, \quad (29)$$

where M_v denotes the cardinality of the constellation used for the SAP with v active subcarriers. Note that JM-OFDM-SNM can be considered as a special case of AJM-OFDM-SNM with $M_1 = M_2 = \dots = M_V$. Obviously, the transmission rate of AJM-OFDM-SNM is given by

$$\bar{r}_{\text{AJM}} = \bar{m} = \lfloor \log_2(\bar{N}_A) \rfloor. \quad (30)$$

TABLE III
TRANSMISSION RATE COMPARISON FOR AJM-OFDM-SNM WITH
 $N = 4$.

V	Symbol Mode	N_A	F	Rate
2	[QPSK, QPSK]	112	64	1.5
2	[BPSK, QPSK]	104	64	1.5
2	[16PSK, BPSK]	88	64	1.5
2	[16PSK, QPSK]	170	128	1.75
2	[8PSK, QPSK]	128	128	1.75
3	[QPSK, QPSK, QPSK]	368	256	2
3	[BPSK, QPSK, BPSK]	136	128	1.75
3	[BPSK, BPSK, QPSK]	288	256	2
3	[BPSK, 8PSK, QPSK]	648	512	2.25

For illustration purposes, we provide an example for AJM-OFDM-SNM with $N = 4$ in Table III. Let us take a look at the case with $N = 4$ and $V = 2$. For demonstrative simplicity, we use [MPSK, MPSK] to represent the JM-OFDM-SNM scheme with $V = 2$ and MPSK modulation, while [M_1 PSK, M_2 PSK] to represent the AJM-OFDM-SNM scheme with $V = 2$ and two different modulation orders M_1 and M_2 (e.g., BPSK for $v = 1$ and QPSK for $v = 2$). To be specific, JM-OFDM-SNM with [QPSK, QPSK] obtains 112 possible transmitted vectors and only 64 transmitted vectors are selected to achieve 1.5 bpcu. Obviously, 48 transmitted vectors are unused and thereby wasted by [QPSK, QPSK]. For AJM-OFDM-SNM with [BPSK, QPSK], 104 transmitted vectors are generated, which still achieves 1.5 bpcu. Compared to JM-OFDM-SNM with [QPSK, QPSK], AJM-OFDM-SNM with [BPSK, QPSK] reduces 6 redundant transmitted vectors, which may improve the BER performance. To further reduce the redundancy of transmitted vectors, AJM-OFDM-SNM with [16PSK, BPSK] is set to have 88 possible transmitted vectors with a transmission rate of 1.5 bpcu. On the other hand, in order to increase the transmission rate, the AJM-OFDM-SNM schemes with [16PSK, QPSK] and [8PSK, BPSK] are proposed to achieve a transmission rate of 1.75 bpcu, which obtain a 1 bpcu increase compared to the JM-OFDM-SNM with [QPSK, QPSK]. To further validate the flexibility of AJM-OFDM-SNM, we investigate more situations for AJM-OFDM-SNM with $N = 4$ and $V = 3$. From Table III, we can see that JM-OFDM-SNM with [QPSK, QPSK, QPSK] only utilizes 256 out of totally 368 transmitted vectors to achieve a transmission rate of 2 bpcu, which throws 112 available transmitted vectors away. To save the SAP resource, we can employ either AJM-OFDM-SNM with [BPSK, QPSK, BPSK] or [BPSK, BPSK, QPSK] to produce 136 or 288 transmitted vectors, respectively, which reduces the redundant transmitted vectors with a transmission rate of 1.75 or 2 bpcu. Besides, AJM-OFDM-SNM with [BPSK, 8PSK, QPSK] is further implemented to increase the transmission rate of up to 2.25 bpcu.

It can be seen from above examples that compared to JM-OFDM-SNM, AJM-OFDM-SNM is able to not only achieve a higher transmission rate but also reduce the number of redundant transmitted vectors by properly adjusting the constellation order for different numbers of active subcarriers. In other words, AJM-OFDM-SNM is more flexible and practical than JM-OFDM-SNM. To clearly exhibit the mapping rule between the input bits and transmitted vectors, let us take AJM-OFDM-SNM with $N = 4$, $V = 2$, and [BPSK, QPSK] as an example, which has 64 legal transmitted vectors and a transmission rate of 1.5 bpcu. Assuming the input bits are (0000), the corresponding transmitted vector is given by $\bar{\mathbf{x}}_1 = [-1, 0, 0, 0]^T$. However, if the input bits are (1111), the transmitted vector is $\bar{\mathbf{x}}_{64} = [0, 0, \frac{1}{\sqrt{2}}(1+j), \frac{1}{\sqrt{2}}(1+j)]^T$. It is easy to find that the modulated symbols in $\bar{\mathbf{x}}_1$ and $\bar{\mathbf{x}}_{64}$ are selected from BPSK and QPSK, respectively.

Remark: In AJM-OFDM-SNM, $C(N, v)$ possible combinations are fully considered with v active subcarriers, which ignores the channel quality of each subcarrier. The flexibility of AJM-OFDM-SNM enables us to further enhance the re-

liability by discarding the combinations containing the weak subchannels and only using the combinations with the strong subchannels (Higher-order modulation can be employed to adapt to the channel as well.), when the channel is available to the transceiver. Due to page limitation, we omit the description of this channel adaptive AJM-OFDM-SNM scheme.

B. JM-OFDM-IQ-SNM

The second enhanced JM-OFDM-SNM scheme, namely JM-OFDM-IQ-SNM, performs indexing independently on the I- and Q- components.

For demonstrative simplicity, we apply two pulse amplitude modulation (PAM) constellations for I- and Q- domains, which stand for the real and imaginary parts of an amplitude-phase modulated symbol, respectively. In JM-OFDM-IQ-SNM, V out of totally N subcarriers are allowed to be activated for the I/Q domain, where $N_T = \sum_{v=1}^V C(N, v)$ SAPs exist for IQ domains. For the I-branch, the number of generated vectors for transmission is given by

$$N_A^I = \sum_{v=1}^V C(N, v)(M_v^I)^v, \quad (31)$$

where M_v^I denotes the constellation order of PAM for the I-branch when activating v subcarriers. Similarly, for the Q-branch, the number of generated vectors for transmission is determined by

$$N_A^Q = \sum_{v=1}^V C(N, v)(M_v^Q)^v, \quad (32)$$

where M_v^Q denotes the constellation order of PAM for the Q-branch when activating v subcarriers. After obtaining the transmitted vectors for both of the IQ components, the total number of possible transmitted vectors for JM-OFDM-IQ-SNM can be calculated as

$$\tilde{N}_A = N_A^I \cdot N_A^Q. \quad (33)$$

Therefore, the transmission rate of JM-OFDM-IQ-SNM is given by

$$\bar{r}_{\text{JM-IQ}} = \tilde{m} = \lfloor \log_2(\tilde{N}_A) \rfloor, \quad (34)$$

and $\tilde{F} = 2^{\lfloor \log_2(\tilde{N}_A) \rfloor}$ vectors are utilized for transmission.

TABLE IV
TRANSMISSION RATE COMPARISON FOR JM-OFDM-IQ-SNM WITH
 $V = 2$ AND $N = 4, 8$.

N	Symbol Mode	\tilde{N}_A	\tilde{F}	Rate
4	I: [2PAM, 2PAM] Q: [2PAM, 2PAM]	1024	1024	2.5
4	[16QAM, 16QAM]	1600	1024	2.5
8	I: [2PAM, 2PAM] Q: [2PAM, 2PAM]	16384	16384	1.75
8	[32QAM, 32QAM]	28928	16384	1.75

For clarity, we provide an example of JM-OFDM-IQ-SNM with $V = 2$ and $N = 4, 8$ in Table IV. It can be seen from

Table IV that JM-OFDM-IQ-SNM with $N = 4$, $V = 2$, and [2PAM, 2PAM] for both of the IQ components obtains 1024 transmitted vector with a transmission rate of 2.5 bpcu, while JM-OFDM-SNM with $N = 4$ and $V = 2$ needs 16QAM for each SAP to achieve the same transmission rate. In addition, JM-OFDM-IQ-SNM with $N = 8$, $V = 2$, and [2PAM, 2PAM] for both IQ components obtains 16384 transmitted vectors with a transmission rate of 1.75 bpcu, while JM-OFDM-SNM with $N = 8$ and $V = 2$ needs 32QAM for each SAP to achieve the same transmission rate. Apparently, JM-OFDM-IQ-SNM is able to employ a lower cardinality of the constellation to achieve the same transmission rate as JM-OFDM-SNM with a larger cardinality. This indicates that JM-OFDM-IQ-SNM may obtain a better BER performance than JM-OFDM-SNM.

C. Low-Complexity Detection for AJM-OFDM-SNM and JM-OFDM-IQ-SNM

The optimal ML detection for AJM-OFDM-SNM and JM-OFDM-IQ-SNM is the same as that of JM-OFDM-SNM (c.f. (8)) by considering all possible transmitted signal vectors, which leads to high detection complexity. Therefore, similar to JM-OFDM-SNM, we also propose LLR detection methods for AJM-OFDM-SNM and JM-OFDM-IQ-SNM, which largely reduce the computational complexity compared to their relative ML detection methods. Since the LLR detection for JM-OFDM-IQ-SNM can be performed in a similar manner to that for AJM-OFDM-SNM, we only shed light on the detection process of AJM-OFDM-SNM and omit that of JM-OFDM-IQ-SNM for brevity.

The LLR metric can be formulated as

$$\begin{aligned} L_{\text{AJM}}(\alpha) &= \ln \frac{\sum_{v=1}^V \Pr(A_\alpha^v | y(\alpha))}{\Pr(\bar{A}_\alpha | y(\alpha))} \\ &= \ln \frac{\sum_{v=1}^V \Pr(A_\alpha^v) f(y(\alpha) | A_\alpha^v)}{\Pr(\bar{A}_\alpha) f(y(\alpha) | \bar{A}_\alpha)}, \end{aligned} \quad (35)$$

where A_α^v denotes the event that the α th subcarrier is active of probability $\Pr(A_\alpha^v) = \frac{v}{N_T} C(N, v)$ for the case of activating v subcarriers with $T = \sum_{v=1}^V C(N, v)$. The conditional PDF $f(y(\alpha) | A_\alpha^v)$ can be expressed in (36), shown at the top of the next page.

Then, by considering all different signal constellations, we can obtain the estimated signal set for the α -th subcarrier as

$$\hat{s}(\alpha) = [\hat{s}_{M_1}(\alpha), \dots, \hat{s}_{M_V}(\alpha)]. \quad (37)$$

To facilitate the signal detection, the optimally estimated symbol for the α -th subcarrier is also reserved as $\hat{s}^\circ(\alpha) \in \hat{s}(\alpha)$ with the minimum Euclidean distance. Therefore, the correspondingly estimated modulated symbol is finally obtained by $\hat{s}_{\text{AJM}} = [\hat{s}^\circ(1), \dots, \hat{s}^\circ(N)]$. Having $\{L_{\text{AJM}}(\alpha)\}_{\alpha=1}^N$ and \hat{s}_{AJM} , the following detection process is the same as that of JM-OFDM-SNM (c.f. (11) and (12)), and the information bits can be easily estimated.

D. Complexity Analysis

To clearly show the effect of the low-complexity detection method, we measure the computational complexity of the low-complexity LLR and the optimal ML detections in terms of

$$f(y(\alpha)|A_\alpha^v) = \begin{cases} \frac{1}{\pi\sigma^2} \exp(-\frac{1}{\sigma^2}|y(\alpha) - \frac{1}{\sqrt{v}}h_\alpha\hat{s}_{M_v}(\alpha)|^2), & \text{if the } \alpha\text{th subcarrier is active,} \\ \frac{1}{\pi\sigma^2} \exp(-\frac{1}{\sigma^2}|y(\alpha)|^2), & \text{if the } \alpha\text{th subcarrier is inactive.} \end{cases} \quad (36)$$

the number of complex multiplications for JM-OFDM-SNM and AJM-OFDM-SNM.

In JM-OFDM-SNM, it is obvious that the computational complexity of the proposed detection method comes from the calculations of the LLR values $\{L(\alpha)\}_{\alpha=1}^N$ in (9) and the estimated SAP \hat{v} . First, calculating $f(y(\alpha)|A_\alpha)$, $f(y(\alpha)|\bar{A}_\alpha)$ and $\Pr(A_\alpha)$ needs $(2M + 10 + V)$ multiplications for a given α . Therefore, obtaining $\{L(\alpha)\}_{\alpha=1}^N$ requires $N(2M + 10 + V)$ multiplications. Second, determining the estimated SAP \hat{v} needs $3NV$ multiplications. Therefore, the total number of multiplications for the proposed LLR detection in JM-OFDM-SNM is $(2MN + 10N + 4NV)$. On the other hand, the total number of complex multiplications for the optimal ML detection in (8) is $3NF$. Similar to JM-OFDM-SNM, the computational complexity of the LLR detection for AJM-OFDM-SNM only depends on the calculations of the LLR values $\{L_{AJM}(\alpha)\}_{\alpha=1}^N$ in (35) and the estimated SAP \hat{v} . For a given v , determining $\Pr(A_\alpha^v)f(y(\alpha)|A_\alpha^v)$ needs $2M_v + 8$ multiplications and thus calculating $\sum_{v=1}^V \Pr(A_\alpha^v)f(y(\alpha)|A_\alpha^v)$ amounts to $8V + 2\sum_{v=1}^V M_v$. Besides, calculating $f(y(\alpha)|\bar{A}_\alpha)$ needs 4 multiplications. Therefore, obtaining $L_{AJM}(\alpha)$ generates $(4 + 8V + 2\sum_{v=1}^V M_v)$ multiplications for a given α , and in total $N(4 + 8V + 2\sum_{v=1}^V M_v)$ multiplications are required for all values of $L_{AJM}(\alpha)$ with $\alpha = 1, \dots, N$. Additionally, $3NV$ multiplications are required for estimating SAP. Hence, the total number of multiplications required by the LLR detection for AJM-OFDM-SNM is $4N + 11NV + 2N\sum_{v=1}^V M_v$, while that for the optimal ML detection is $3NU$ with $U = 2^{\lceil \log_2 N_A \rceil}$. Note that the computational complexity of the optimal ML detection for the conventional OFDM scheme is given by $2NM$, which is even less than that of the LLR detection for (A)JM-OFDM-SNM. However, as will be verified in Section VI, the conventional OFDM scheme performs worse than (A)JM-OFDM-SNM. This means (A)JM-OFDM-SNM can strike an interesting trade-off between the error performance and computational complexity.

TABLE V
COMPUTATIONAL COMPLEXITY COMPARISON OF DETECTION METHODS FOR JM-OFDM-SNM.

Rate	(N, V, M)	Proposed	ML	Reduction
1.25	(4, 2, 2)	88	384	77%
2	(4, 3, 4)	120	3072	96%
1.125	(8, 3, 2)	208	12288	98%
1.75	(8, 4, 4)	272	393216	99%

For better illustration, we present the computational complexity comparison of LLR and ML detections for JM-OFDM-SNM in Table V. To be specific, the ML detection requires 384 multiplications while the LLR detection only needs 88

multiplications, which attains a complexity reduction of 77% for JM-OFDM-SNM with $N = 4$ and $V = M = 2$. Keeping increasing V and M , a reduction of 96% is achieved by the LLR detection for JM-OFDM-SNM with $N = 4$, $V = 3$ and $M = 4$. In addition, the LLR detection achieves reductions of 98% and 99% for JM-OFDM-SNM with $N = 8$, $V = 3$, and $M = 4$, and JM-OFDM-SNM with $N = 8$ and $V = M = 4$, respectively. It can be concluded from above that the computational complexity is largely reduced by the LLR detection, especially for large values of N , V , and M .

TABLE VI
COMPUTATIONAL COMPLEXITY COMPARISON OF DETECTION METHODS FOR AJM-OFDM-SNM.

Rate	$(N, V, [M_1, \dots, M_V])$	Proposed	ML	Reduction
3	(2, 2, [8, 8])	116	384	69%
2	(4, 3, [2, 2, 4])	212	3072	93%
1	(8, 2, [2, 4])	304	6144	95%

The comparison of LLR and ML detections for AJM-OFDM-SNM in terms of computational complexity is also considered in Table VI at the same SEs. Specifically, AJM-OFDM-SNM with $N = 2$, $V = 2$, and $M_1 = M_2 = 8$ at an SE of 3 bpcu requires 116 and 384 multiplications for LLR and ML detections, respectively. Obviously, the LLR detection has a lower computational complexity than the ML detection. On the other hand, AJM-OFDM-SNM with $N = 4$, $V = 3$, $M_1 = M_2 = 2$, and $M_3 = 4$ at an SE of 2 bpcu requires 212 and 3072 multiplications for the LLR and ML detections, respectively. In addition, the ML detection for AJM-OFDM-SNM with $N = 8$, $V = 2$, $M_1 = 2$ and $M_2 = 4$ at an SE of 1 bpcu requires 6144 multiplications, while the LLR detection with $N = 8$, $V = 2$, $M_1 = 2$ and $M_2 = 4$ needs only 304 multiplications, which leads to a great reduction of computational complexity.

VI. SIMULATION RESULTS

In this section, we perform computer simulations to evaluate the BER performance of JM-OFDM-SNM, AJM-OFDM-SNM, and JM-OFDM-IQ-SNM under the assumption of Rayleigh fading channels and perfect channel estimation. For convenience, we adopt the shorthands “JM-SNM, $(N, V, M\text{PSK/QAM})$ ” for the JM-OFDM-SNM scheme with N subcarriers, V maximal active subcarriers, and the M -ary PSK/QAM constellation, “AJM-SNM, $(N, V, [M_1\text{PSK/QAM}, \dots, M_V\text{PSK/QAM}])$ ” for the AJM-OFDM-SNM scheme with N subcarriers, V maximal active subcarriers, and V signal constellations, “JM-IQ-SNM, $(N, V, [M_1^I\text{PAM}, \dots, M_V^I\text{PAM}], [M_1^Q\text{PAM}, \dots, M_V^Q\text{PAM}])$ ” for the JM-OFDM-IQ-SNM scheme with N subcarriers, V maximal active subcarriers, and V PAM constellations for the I-branch component,

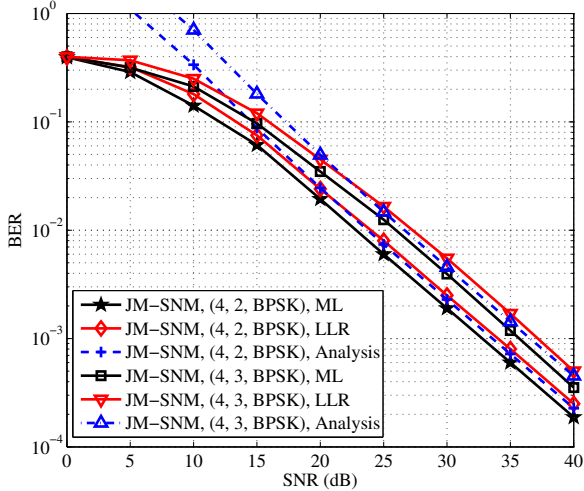


Fig. 2. Performance comparison between the optimal ML detection and the proposed low-complexity LLR detection for JM-OFDM-SNM with $N = 4$.

and another V PAM constellations for the Q-branch component, and “OFDM, (N , M PSK/QAM)” for the conventional OFDM scheme with N subcarriers and M -ary PSK/QAM constellation.

In Fig. 2, we compare the BER performance between the optimal ML detection and the proposed low-complexity LLR detection for “JM-SNM (4, 2, BPSK)” and “JM-SNM (4, 3, BPSK)”. It can be seen from Fig. 2 that the proposed LLR detection approaches the ML detection with an acceptable performance loss. To be specific, the performance gap between the LLR detection and ML detection is about 1 dB over the entire SNR region for both “JM-SNM (4, 2, BPSK)” and “JM-SNM (4, 3, BPSK)”. Note that the small performance loss stems from the erroneous estimation on the number of active subcarriers \hat{v} . In Fig. 2, we also plot the BER curves from the theoretical analysis. It can be found that the theoretical curves of both “JM-SNM (4, 2, BPSK)” and “JM-SNM (4, 3, BPSK)” well match the simulation curves in the high SNR region. The convergence validates our performance analysis presented in Section IV.

In Fig. 3, we compare the block error ratio (BLER) performance of (A)JM-OFDM-SNM and OFDM-SNM with $N = 4, 8$. Since it is difficult to make a fair comparison between JM-OFDM-SNM and OFDM-SNM at the same transmission rate, we alternatively select the AJM-OFDM-SNM for comparison with OFDM-SNM. Specifically, we draw the BLER curves of “AJM-SNM, (4, 2, [8PSK, QPSK])” ($V = 2$), and OFDM-SNM with $N = 4$ and QPSK at the same transmission rate of 1.75 bpcu in Fig. 3(a). It can be seen that “AJM-SNM, (4, 2, [8PSK, QPSK])” obtains a 2 dB SNR gain over OFDM-SNM with $N = 4$ and QPSK in the region of $\text{SNR} > 25$ dB. To further examine the performance of AJM-OFDM-SNM with a different value of V , we also examine the BLER performance of “AJM-SNM, (4, 3, [BPSK, QPSK, BPSK])” ($V = 3$) at the same transmission rate in the figure. It can be observed that “AJM-SNM, (4, 3, [BPSK, QPSK, BPSK])” still outperforms OFDM-SNM with $N = 4$ and QPSK with a

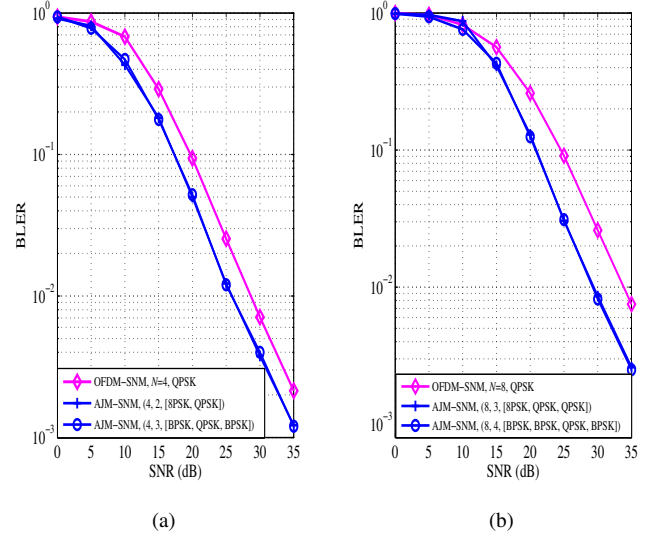


Fig. 3. Performance comparison between OFDM-SNM and AJM-OFDM-SNM. (a) 1.75 bpcu; (b) 1.5 bpcu.

2 dB SNR gain. We then increase N from 4 to 8 and compare the BLER performance of “AJM-SNM, (8, 3, [8PSK, QPSK, QPSK])”, “AJM-SNM, (8, 4, [BPSK, BPSK, QPSK, BPSK])”, and OFDM-SNM with $N = 8$ and QPSK at a transmission rate of 1.5 bpcu in Fig. 3(b). From Fig. 3(b), we observe that both “AJM-SNM, (8, 3, [8PSK, QPSK, QPSK])” and “AJM-SNM, (8, 4, [BPSK, BPSK, QPSK, BPSK])” achieve better performance almost over the entire SNR region with a constant 4 dB SNR gain for $\text{SNR} \geq 20$ dB, which further validates the performance advantage of (A)JM-OFDM-SNM. Interestingly, we can see from Fig. 3 that “AJM-SNM, (4, 2, [8PSK, QPSK])” and “AJM-SNM, (8, 3, [8PSK, QPSK, QPSK])” achieve almost the same BLER performance as “AJM-SNM, (4, 3, [BPSK, QPSK, BPSK])” and “AJM-SNM, (8, 4, [BPSK, BPSK, QPSK, BPSK])” in the high SNR region. These phenomena can be explained by the fact that the SAP in AJM-OFDM-SNM is likely to be correctly estimated, while the detection error only occurs in the estimation of modulated symbols.

In Fig. 4, we compare the BER performance of (A)JM-OFDM-SNM and OFDM. From Fig. 4, we can see that “JM-SNM, (2, 2, 8QAM)” achieves an up to 1 dB SNR gain over “OFDM, (2, 8QAM)” at the same transmission rate of 3 bpcu. Similarly for the same transmission rate of 4 bpcu, “AJM-SNM, (2, 2, [2QAM, 16QAM])” outperforms “OFDM, (2, 16QAM)” attaining an up to 0.8 dB SNR gain. In addition, “AJM-SNM, (2, 2, [2PSK, 16PSK])” still obtains almost 1 dB SNR gain over “OFDM, (2, 16PSK)”. From above, the superiority of our proposed (A)JM-OFDM-SNM scheme over the conventional OFDM scheme is verified.

Figure 5 shows the BER performance of (A)JM-OFDM-SNM with $N = 4$ and $V = 2$. With respect to “AJM-SNM, (4, 2, [BPSK, QPSK])” with a transmission rate of 6 bpcu, “JM-SNM, (4, 2, QPSK)” with a transmission rate of 1.5 bpcu, and “AJM-SNM, (4, 2, [8PSK, QPSK])” with a transmission rate of 1.75 bpcu, It can be observed that “AJM-SNM, (4, 2,

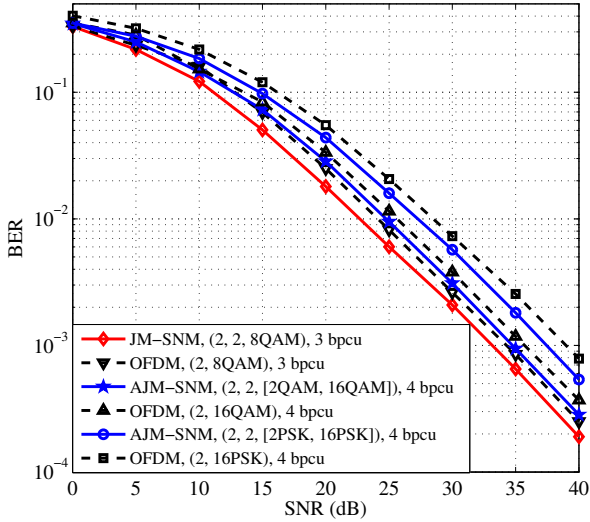


Fig. 4. Performance comparison of (A)JM-OFDM-SNM and OFDM with different configurations.

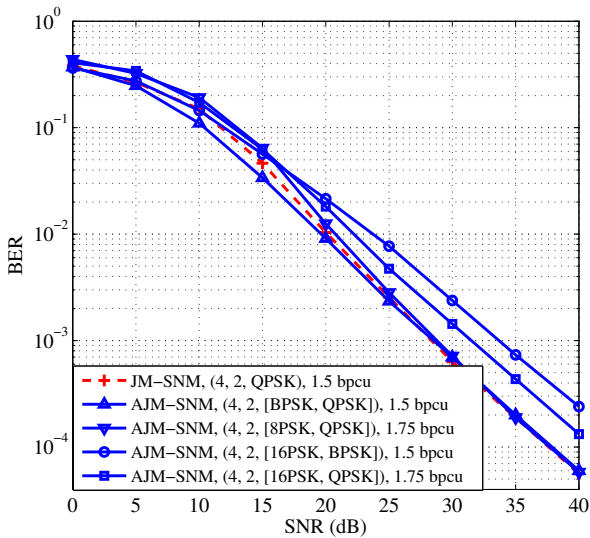


Fig. 5. Performance comparison for AJM-OFDM-SNM with $N = 4$ and $V = 2$.

[BPSK, QPSK]” with 1.5 bpcu performs the best and “AJM-SNM, (4, 2, [8PSK, QPSK])” with 1.75 bpcu performs the worst in the low SNR region. However, they achieve almost the same performance in the high SNR region. This is because the SAP and the modulated symbol are prone to detection errors in the low SNR region, such that 8PSK in “AJM-SNM, (4, 2, [8PSK, QPSK])” and BPSK in “AJM-SNM, (4, 2, [BPSK, QPSK])” lead to the worst and best performance, respectively. However, the SAP and modulated symbols are immune to detection errors in the high SNR region. Note that the majority of transmitted vectors in “AJM-SNM, (4, 2, [BPSK, QPSK])”, “JM-SNM, (4, 2, QPSK)”, and “AJM-SNM, (4, 2, [8PSK, QPSK])” are dominated by QPSK with $v = 2$ (96 possible transmitted vectors exist), and only a small portion of

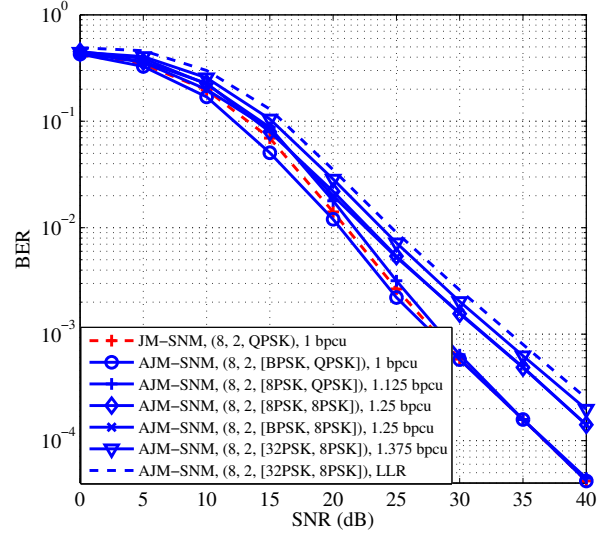


Fig. 6. Performance comparison for AJM-OFDM-SNM with $N = 8$ and $V = 2$.

transmitted vectors are generated by BPSK/QSPK/8PSK with $v = 1$ (see Table III). Therefore, although “AJM-SNM, (4, 2, [8PSK, QPSK])” has a larger transmission rate, all three AJM-OFDM-SNM schemes achieve almost the same BER performance in the high SNR region. This is because the transmitted vectors with QPSK and $v = 2$ play a major role on the BER performance in the high SNR region. In addition, we show the simulation results for “AJM-SNM, (4, 2, [16PSK, BPSK])” with 1.5 bpcu and “AJM-SNM, (4, 2, [16PSK, QPSK])” with 1.75 bpcu. It can be seen that “AJM-SNM, (4, 2, [16PSK, BPSK])” leads to a better BER performance than “AJM-SNM, (4, 2, [16PSK, QPSK])” in the low SNR region, but worse BER performance in the high SNR region. This can be understood by the fact that the transmit vectors with QPSK and $v = 2$ are dominant in all available vectors for “AJM-SNM, (4, 2, [16PSK, QPSK])”, while the transmit vectors with 16PSK and $v = 1$ are dominant for “AJM-SNM, (4, 2, [16PSK, BPSK])”, which leads to a better performance in the high SNR region for “AJM-SNM, (4, 2, [16PSK, QPSK])”.

To further confirm our observation, in Fig. 6 we compare the BER performance of (A)JM-OFDM-SNM with $N = 8$ and $V = 2$. From Fig. 6, one can still find that “AJM-SNM, (8, 2, [BPSK, QPSK])” with 1 bpcu, “JM-SNM, (8, 2, QPSK)” with 1 bpcu, and “AJM-SNM, (8, 2, [8PSK, QPSK])” with 1.125 bpcu achieve almost the same BER performance in the high SNR region because of the dominating transmit vectors with QPSK and $v = 2$. Similarly, “AJM-SNM, (8, 2, [8PSK, 8PSK])” and “AJM-SNM, (8, 2, [BPSK, 8PSK])” both with 1.275 bpcu achieve the same BER performance in the high SNR region, which is dominated by 8PSK with $v = 2$. Besides, “AJM-SNM, (8, 2, [32PSK, 8PSK])” with 1.375 bpcu achieves the worst BER performance since the number of transmitted vectors with 32PSK and $v = 1$ is non-negligible, which degrades the system performance. On the other hand, the proposed low-complexity LLR detection approaches the optimal ML detection with a tolerably small performance loss

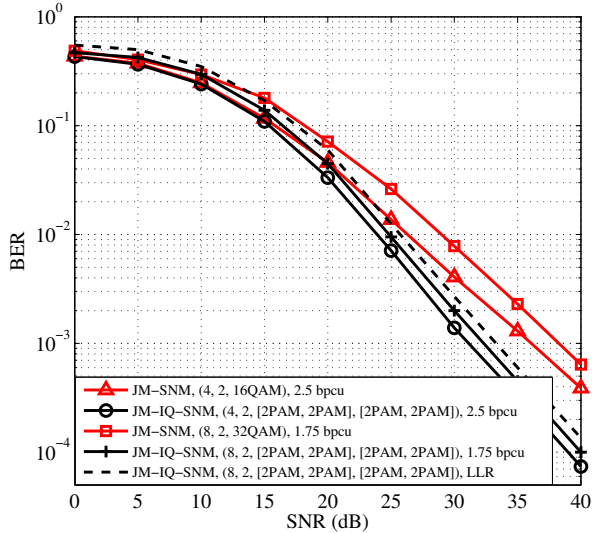


Fig. 7. Performance comparison for JM-OFDM-SNM and JM-OFDM-IQ-SNM with different configurations.

for “AJM-SNM, (8, 2, [32PSK, 8PSK])”. From above, we can summarize that AJM-OFDM-SNM can not only increase the length of input bits, but also improve the BER performance by properly adjusting the constellation cardinality.

To evaluate the BER performance of JM-OFDM-IQ-SNM, we draw the simulation curves for “JM-IQ-SNM, (4, 2, [2PAM, 2PAM], [2PAM, 2PAM])” with 2.5 bpcu, “JM-IQ-SNM, (8, 2, [2PAM, 2PAM], [2PAM, 2PAM])” with 1.75 bpcu, “JM-SNM, (4, 2, 16QAM)” with 2.5 bpcu, and “JM-SNM, (8, 2, 32QAM)” with 1.75 bpcu in Fig. 7. We can see from Fig. 7 that “JM-IQ-SNM, (4, 2, [2PAM, 2PAM], [2PAM, 2PAM])” significantly outperforms “JM-SNM, (4, 2, 16QAM)”, achieving a 5 dB SNR gain at a BER level of 10^{-3} . This is because 2PAM is employed in the JM-OFDM-IQ-SNM scheme, while 16QAM with a much larger Euclidean distance is adopted in the JM-OFDM-SNM scheme to achieve the transmission rate of 2.5 bpcu. We can also find that “JM-IQ-SNM, (8, 2, [2PAM, 2PAM], [2PAM, 2PAM])” achieves better performance than “JM-SNM, (8, 2, 32QAM)” with a 6 dB SNR gain due to the poor performance of 32QAM in “JM-SNM, (8, 2, 32QAM)”. It should be noted that JM-OFDM-IQ-SNM obtains excellent performance because there exist a large number of available candidates of transmitted vectors generated by lower-order modulation schemes, e.g., 2PAM. Additionally, the simulation curve of the proposed low-complexity detection approaches that of the optimal ML detection with a small gap for “JM-IQ-SNM, (8, 2, [2PAM, 2PAM], [2PAM, 2PAM])”.

The achievable rates of “AJM-SNM, (4, 2, [8PSK, QPSK])”, “AJM-SNM, (8, 3, [BPSK, QPSK, QPSK])”, “OFDM-SNM, (4, QPSK)”, “OFDM-SNM, (8, QPSK)”, and “JM-IQ-SNM, (8, 2, [2PAM, 2PAM], [2PAM, 2PAM])” are presented in Fig. 8. It can be seen from Fig. 8 that the achievable rates of all schemes increase with the increase of SNR and approach to constants at high SNR. This is because less detection errors

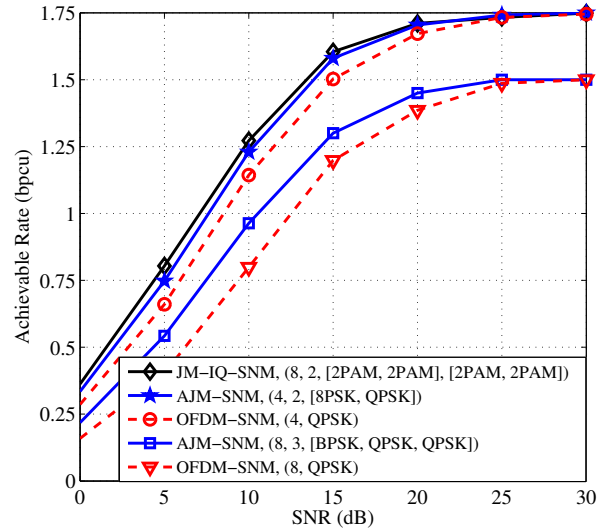


Fig. 8. Achievable rate comparison between AJM-OFDM-SNM and OFDM-SNM schemes.

occur at the receiver as SNR increases and the information bits are correspondingly estimated with less errors. More importantly, although the SEs for all schemes tend to saturate at high SNR, we still can see from Fig. 8 that “JM-IQ-SNM, (8, 2, [2PAM, 2PAM], [2PAM, 2PAM])” with a transmission rate of 1.75 bpcu, “AJM-SNM, (4, 2, [8PSK, QPSK])” with a transmission rate of 1.75 bpcu, and “AJM-SNM, (8, 3, [BPSK, QPSK, QPSK])” with a transmission rate of 1.5 bpcu outperform “OFDM-SNM, (4, QPSK)” with a transmission rate of 1.75 bpcu and “OFDM-SNM, (8, QPSK)” with a transmission rate of 1.5 bpcu at low-to-medium SNRs, which further reveals the advantages of our proposed scheme.

VII. CONCLUSIONS

In this paper, we proposed the JM-OFDM-SNM scheme to obtain better performance than OFDM-SNM by jointly considering the SAPs and modulated symbols for different numbers of active subcarriers. An LLR detection method for JM-OFDM-SNM was proposed, which achieves very close performance to the optimal ML detection over the entire SNR region. In addition, we derived the upper bound on the BER and the lower bound on the achievable rate of JM-OFDM-SNM. To further enhance the utilization of frequency resource, we proposed AJM-OFDM-SNM and JM-OFDM-IQ-SNM to improve the SE and the error performance of JM-OFDM-SNM, where AJM-OFDM-SNM adjusts the constellation orders for different numbers of active subcarriers, and JM-OFDM-IQ-SNM obtains a larger number of transmitted vectors. By computer simulations, we showed that both AJM-OFDM-SNM and JM-OFDM-IQ-SNM outperform JM-OFDM-SNM under the same transmission rate.

REFERENCES

- [1] S. Dang, O. Amin, B. Shihada, and M.-S. Alouini, “What should 6G be?,” *Nature Electronics*, vol. 3, pp. 20-29, Jan. 2020.

- [2] E. Basar, M. Wen, R. Mesleh, M. Di Renzo, Y. Xiao, and H. Haas, "Index modulation techniques for next-generation wireless networks," *IEEE Access*, vol. 5, pp. 16693-16746, 2017.
- [3] A. M. Jaradat, J. M. Hamamreh, and H. Arslan, "Modulation options for OFDM-based waveforms: Classification, comparison, and future directions," *IEEE Access*, vol. 7, pp. 17263-17278, 2019.
- [4] S. Dogan, A. Tusha, E. Basar, and H. Arslan, "Multidimensional index modulation for 5G and beyond wireless networks," 2020. [Online]. Available: <https://arxiv.org/pdf/2010.00850.pdf>
- [5] M. Wen, B. Zheng, K. J. Kim, M. Di Renzo, T. A. Tsiftsis, K.-C. Chen, and N. Al-Dhahir, "A survey on spatial modulation in emerging wireless systems: Research progresses and applications," *IEEE J. Sel. Areas Commun.*, vol. 37, no. 9, pp. 1949-1972, Sept. 2019.
- [6] N. Ishikawa, S. Sugiura, and L. Hanzo, "50 years of permutation, spatial and index modulation: From classical RF to visible light communications and data storage," *IEEE Commun. Surveys Tuts.*, vol. 20, No. 3, pp. 1905-1938, 3rd Quart. 2018.
- [7] T. Mao, Q. Wang, Z. Wang, and S. Chen, "Novel index modulation techniques: A survey," *IEEE Commun. Surveys Tuts.*, vol. 21, no. 1, pp. 315-348, 1st Quart. 2019.
- [8] R. Mesleh, H. Haas, S. Sinanovic, C. W. Ahn, and S. Yun, "Spatial modulation," *IEEE Trans. Veh. Technol.*, vol. 57, no. 4, pp. 2228-2241, July 2008.
- [9] J. Jeganathan, A. Ghrayeb, L. Szczecinski, and A. Ceron, "Space shift keying modulation for MIMO channels," *IEEE Trans. Wireless Commun.*, vol. 8, no. 7, pp. 3692-3703, July 2009.
- [10] A. Younis, N. Serafimovski, R. Mesleh, and H. Haas, "Generalised spatial modulation," in *Proc. 2010 Conf. Record of the 44th Asilomar Conf. on Signals, Syst. and Comput.*, Pacific Grove, CA, USA, Nov. 2010, pp. 1498-1502.
- [11] J. Wang, S. Jia, and J. Song, "Generalised spatial modulation system with multiple active transmit antennas and low complexity detection scheme," *IEEE Trans. Wireless Commun.*, vol. 11, no. 4, pp. 1605-1615, Apr. 2012.
- [12] J. Jeganathan, A. Ghrayeb, and L. Szczecinski, "Generalized space shift keying modulation for MIMO channels," in *Proc. IEEE 19th Int. Symp. Personal, Indoor and Mobile Radio Commun. (PIMRC)*, Cannes, France, Sep. 2008, pp. 1-5.
- [13] R. Mesleh, *et al.*, "Quadrature spatial modulation," *IEEE Trans. Veh. Technol.*, vol. 64, no. 6, pp. 2738-2742, June 2015.
- [14] J. M. Hamamreh, *et al.*, "Multiple input multiple output with antenna number modulation and adaptive antenna selection," *RS Open J. Innov. Commun. Technol.*, vol. 4, pp. 1-14, June 2020.
- [15] L. Yang, "Transmitter preprocessing aided spatial modulation for multiple-input multiple-output systems," in *Proc. IEEE Veh. Techn. Conf. (VTC Spring)*, Budapest, Hungary, May 2011, pp. 1-5.
- [16] R. Zhang, L. Yang, and L. Hanzo, "Generalised pre-coding aided spatial modulation," *IEEE Trans. Wireless Commun.*, vol. 12, no. 11, pp. 5434-5443, Nov. 2013.
- [17] A. Stavridis *et al.*, "Performance analysis of multi-stream receive spatial modulation in the MIMO broadcast channel," *IEEE Trans. Wireless Commun.*, vol. 15, no. 3, pp. 1808-1820, Mar. 2016.
- [18] J. Li, M. Wen, X. Cheng, Y. Yan, S. Song, and M. H. Lee, "Generalised pre-coding aided quadrature spatial modulation," *IEEE Trans. Veh. Technol.*, vol. 66, no. 2, pp. 1881-1886, Feb. 2017.
- [19] E. Basar, U. Aygolu, E. Panayirci, and H. V. Poor, "Orthogonal frequency division multiplexing with index modulation," *IEEE Trans. Signal Process.*, vol. 61, no. 22, pp. 5536-5549, Nov. 2013.
- [20] Y. Xiao, S. Wang, L. Dan, X. Lei, P. Yang, and W. Xiang, "OFDM with interleaved subcarrier-index modulation," *IEEE Commun. Lett.*, vol. 18, no. 8, pp. 1447-1450, Aug. 2014.
- [21] M. Wen, X. Cheng, M. Ma, B. Jiao, and H. V. Poor, "On the achievable rate of OFDM with index modulation," *IEEE Trans. Signal Process.*, vol. 64, no. 8, pp. 1919-1932, Apr. 2016.
- [22] M. Wen, B. Ye, E. Basar, Q. Li, and F. Ji, "Enhanced orthogonal frequency division multiplexing with index modulation," *IEEE Trans. Wireless Commun.*, vol. 16, no. 7, pp. 4786-4801, July 2017.
- [23] A. I. Siddiq, "Low complexity OFDM-IM detector by encoding all possible subcarrier activation patterns," *IEEE Commun. Lett.*, vol. 20, no. 3, pp. 446-449, Mar. 2016.
- [24] R. Fan, Y. J. Yu, and Y. L. Guan, "Generalization of orthogonal frequency division multiplexing with index modulation," *IEEE Trans. Wireless Commun.*, vol. 14, no. 10, pp. 5350-5359, Oct. 2015.
- [25] J. Li, S. Dang, M. Wen, X.-Q. Jiang, Y. Peng, and H. Hai, "Layered orthogonal frequency division multiplexing with index modulation," *IEEE Syst. J.*, vol. 13, no. 4, pp. 3793-3802, Dec. 2019.
- [26] E. Basar, "On multiple-input multiple-output OFDM with index modulation for next generation wireless networks," *IEEE Trans. Signal Process.*, vol. 64, no. 15, pp. 3868-3878, Aug. 2016.
- [27] T. Mao *et al.*, "Dual-mode index modulation aided OFDM," *IEEE Access*, vol. 5, pp. 50-60, 2017.
- [28] T. Mao, Q. Wang, and Z. Wang, "Generalized dual-mode index modulation aided OFDM," *IEEE Commun. Lett.*, vol. 21, no. 4, pp. 761-764, Apr. 2017.
- [29] M. Wen, E. Basar, Q. Li, B. Zheng, and M. Zhang, "Multiple-mode orthogonal frequency division multiplexing with index modulation," *IEEE Trans. Commun.*, vol. 65, no. 9, pp. 3892-3906, Sep. 2017.
- [30] M. Wen, Q. Li, E. Basar, and W. Zhang, "Generalized multiple-mode OFDM with index modulation," *IEEE Trans. Wireless Commun.*, vol. 17, no. 10, pp. 6531-6543, Oct. 2018.
- [31] J. M. Hamamreh and A. Hajar, "The generalization of orthogonal frequency division multiplexing with subcarrier power modulation to quadrature signal constellations," *RS Open J. Innov. Commun. Technol.*, vol. 4, pp. 1-15, May 2020.
- [32] J. M. Hamamreh and M. Abewa, "Non-coherent OFDM-subcarrier power modulation for low complexity and high throughput IoT applications," *RS Open J. Innov. Commun. Technol.*, vol. 4, pp. 1-13, July, 2020.
- [33] J. Crawford, E. Chatziantoniou, and Y. Ko, "On the SEP analysis of OFDM index modulation with hybrid low complexity greedy detection and diversity reception," *IEEE Trans. Veh. Technol.*, vol. 66, no. 9, pp. 8103-8118, Sep. 2017.
- [34] B. Zheng, M. Wen, E. Basar, and F. Chen, "Multiple-input multiple-output OFDM with index modulation: Low-complexity detector design," *IEEE Trans. Signal Process.*, vol. 65, no. 11, pp. 2758-2772, June 2017.
- [35] J. Li, Q. Li, S. Dang, M. Wen, X.-Q. Jiang, and Y. Peng, "Low-complexity detection for index modulation multiple access," *IEEE Wireless Commun. Lett.*, vol. 9, no. 7, pp. 943-947, July 2020.
- [36] A. M. Jaradat, J. M. Hamamreh, and H. Arslan, "OFDM with subcarrier number modulation," *IEEE Wireless Commun. Lett.*, vol. 7, no. 6, pp. 914-917, Dec. 2018.
- [37] S. Dang, G. Ma, B. Shihada, and M.-S. Alouini, "Enhanced orthogonal frequency-division multiplexing with subcarrier number modulation," *IEEE Internet Things J.*, vol. 6, no. 5, pp. 7907-7920, Oct. 2018.
- [38] A. M. Jaradat *et al.*, "OFDM with hybrid number and index modulation," *IEEE Access*, vol. 8, pp. 55042-55053, 2020.
- [39] M. Chiani and D. Dardari, "Improved exponential bounds and approximation for the Q-function with application to average error probability computation," in *Proc. IEEE Global Telecommun. Conf.*, Bologna, Italy, Nov. 2002, pp. 1399-1402.
- [40] J. G. Proakis, *Digital Communications*, 3rd ed. New York: McGraw-Hill, 1995.
- [41] M.-S. Alouini and A. J. Goldsmith, "A unified approach for calculating error rates of linearly modulated signals over generalized fading channels," *IEEE Trans. Commun.*, vol. 47, no. 9, pp. 1324-1334, Sep. 1999.



Miaowen Wen (SM'18) received the Ph.D. degree from Peking University, Beijing, China, in 2014. From 2019 to 2021, he was with the Department of Electrical and Electronic Engineering, The University of Hong Kong, Hong Kong, as a Post-Doctoral Research Fellow. He is currently an Associate Professor with South China University of Technology, Guangzhou, China. He has published two books and more than 110 journal papers. His research interests include a variety of topics in the areas of wireless and molecular communications.

Dr. Wen was a recipient of the IEEE ComSoc Asia-Pacific Outstanding Young Researcher Award in 2020, and four Best Paper Awards from the IEEE ITST'12, the IEEE ITSC'14, the IEEE ICNC'16, and the IEEE ICST'19. He was the winner in data bakeoff competition (Molecular MIMO) at IEEE Communication Theory Workshop (CTW) 2019, Selfoss, Iceland. He served as a Guest Editor for the IEEE JOURNAL ON SELECTED AREAS IN COMMUNICATIONS and for the IEEE JOURNAL OF SELECTED TOPICS IN SIGNAL PROCESSING. Currently, he is serving as an Editor for the IEEE TRANSACTIONS ON COMMUNICATIONS, the IEEE TRANSACTIONS ON MOLECULAR, BIOLOGICAL, AND MULTI-SCALE COMMUNICATIONS, and the IEEE COMMUNICATIONS LETTERS, and a Guest Editor for the IEEE JOURNAL OF SELECTED TOPICS IN SIGNAL PROCESSING (Special Issue on Advanced Signal Processing for Local and Private 5G Networks).



Jun Li (S'13-M'17) received the Ph.D. degrees from Chonbuk National University, Jeonju, South Korea, in 2016. He is currently an Associate Professor with Guangzhou University, Guangzhou, China. He serves as a reviewer for IEEE TRANSACTIONS ON COMMUNICATIONS, IEEE TRANSACTIONS ON WIRELESS COMMUNICATIONS, IEEE JOURNAL ON SELECTED AREAS IN COMMUNICATIONS, IEEE TRANSACTIONS ON INTELLIGENT TRANSPORTATION SYSTEMS, and IEEE TRANSACTIONS ON VEHICULAR TECHNOLOGY. His research inter-

ests include spatial modulation, OFDM with index modulation, and reconfigurable intelligent surface.



Shuping Dang (S'13-M'18) received B.Eng (Hons) in Electrical and Electronic Engineering from the University of Manchester (with first class honors) and B.Eng in Electrical Engineering and Automation from Beijing Jiaotong University in 2014 via a joint '2+2' dual-degree program. He also received D.Phil in Engineering Science from University of Oxford in 2018. Dr. Dang joined in the R&D Center, Huanan Communication Co., Ltd. after graduating from University of Oxford and is currently working as a Postdoctoral Fellow with the Computer, Elec-

trical and Mathematical Science and Engineering Division, King Abdullah University of Science and Technology (KAUST). He is a co-recipient of the best Paper Award for work presented at 2019 19th IEEE International Conference on Communication Technology. Dr. Dang is also recognized as the Exemplary Reviewer of IEEE COMMUNICATIONS LETTERS in 2019. His current research interests include novel modulation schemes, cooperative communications, terahertz communications, and 6G wireless network design.



Qiang Li (M'20) received the Ph.D. degree from South China University of Technology, Guangzhou, China, in 2020. From 2018 to 2019, he was a Visiting Student Research Collaborator with Princeton University, Princeton, NJ, USA. Since 2020, he has been a faculty member with the Jinan University, Guangzhou, China. His current research interests include index modulation, non-orthogonal multiple access, and reconfigurable intelligent surfaces. He was a recipient of the Excellent Doctoral Dissertation Award from the China Education Society of Electronics and a recipient of the Best Paper Award from the IEEE International Conference on Communication Technology in 2019.



Shahid Mumtaz (SM'16) received the masters and Ph.D. degrees in electrical and electronic engineering from the Blekinge Institute of Technology, Karlskrona, Sweden, and University of Aveiro, Aveiro, Portugal, in 2006 and 2011, respectively. Since 2011, he has been with the Instituto de Telecomunicacoes, Aveiro, Portugal, where he currently holds the position of Auxiliary Researcher and adjunct positions with several universities across the Europe-Asian Region. He is currently a Visiting Researcher with Nokia Bell Labs, Murray Hill, NJ, USA. He is the

author of 4 technical books, 12 book chapters, and more than 150 technical papers in the area of mobile communications.



Huseyin Arslan (IEEE Fellow, IEEE Distinguished Lecturer) received his BS degree from the Middle East Technical University (METU), Ankara, Turkey in 1992; his MS and Ph.D. degrees were received respectively in 1994 and 1998 from Southern Methodist University (SMU), Dallas, TX. From January 1998 to August 2002, he was with the research group of Ericsson, where he was involved with several projects related to 2G and 3G wireless communication systems. Since August 2002, he has been with the Electrical Engineering Department, at

the University of South Florida, where he is a Professor. In December 2013, he joined Istanbul Medipol University to found the Engineering College, where he has worked as the Dean of the School of Engineering and Natural Sciences. In addition, he has worked as a part-time consultant for various companies and institutions including Anritsu Company and The Scientific and Technological Research Council of Turkey.

Dr. Arslan conducts research in wireless systems, with emphasis on the physical and medium access layers of communications. His current research interests are on 5G and beyond radio access technologies, physical layer security, interference management (avoidance, awareness, and cancellation), cognitive radio, multi-carrier wireless technologies (beyond OFDM), dynamic spectrum access, co-existence issues, non-terrestrial communications (High Altitude Platforms), joint radar (sensing) and communication designs. Dr. Arslan has been collaborating extensively with key national and international industrial partners and his research has generated significant interest in companies such as InterDigital, Anritsu, NTT DoCoMo, Raytheon, Honeywell, Keysight technologies. Collaborations and feedback from industry partners has significantly influenced his research. In addition to his research activities, Dr. Arslan has also contributed to wireless communication education. He has integrated the outcomes of his research into education which lead him to develop a number of courses at the University of South Florida. He has developed a unique Wireless Systems Laboratory course (funded by the National Science Foundation and Keysight technologies) where he was able to teach not only the theory but also the practical aspects of wireless communication system with the most contemporary test and measurement equipment.

Dr. Arslan has served as general chair, technical program committee chair, session and symposium organizer, workshop chair, and technical program committee member in several IEEE conferences. He is currently a member of the editorial board for the IEEE Surveys and Tutorials and the Sensors Journal. He has also served as a member of the editorial board for the IEEE Transactions on Communications, the IEEE Transactions on Cognitive Communications and Networking (TCCN), and several other scholarly journals by Elsevier, Hindawi, and Wiley Publishing.